Experimentation and modeling of inclined ballistic impact in thick polycarbonate plates

A. Dorogoy[(1*)], D. Rittel[(1)] and A. Brill[(2)]

(1) Faculty of Mechanical Engineering, Technion – Israel Institute of Technology, 32000, Haifa, Israel.

(2) RAFAEL, P.O. Box 2250, Haifa, Israel

ABSTRACT

The penetration and perforation of a thick polycarbonate (PC) plate (one and 3 stacked) by an armor piercing 7.62 mm projectile is investigated experimentally and numerically. The characteristic structure of the projectile's trajectory in the PC plates is studied. It is observed that the trajectory consist of a cavity and a circumferential cracked zone attached to it, which is fully embedded within a cylindrical plastic zone. The size of the plastic zone is approximately twice that of the cavity zone and can be clearly observed due to the change of the refractive properties of the material. Strong local recovery of the PC is shown as well.

A 3D transient non linear adiabatic finite element simulation is performed using the commercial software Abaqus 6.9 EF1. The numerical analyses include two combined failure criteria: Ductile failure with damage evolution, and tensile failure. The material properties are strain rate and temperature dependent. The numerical simulations are tested by comparing the numerical trajectory prediction to actual trajectories of inclined impacts of projectiles. It is found that the projectile perforates the plate at angles of inclinations of 30^{o} and higher. The observed agreement between experiments and numerical modeling indicates that the combined effect of the two failure criteria (tensile vs. ductile failure) can reasonably well predict the projectile's trajectory within a thick PC plate.

The numerical analyses are further used to study the effect of the projectile impact velocity on the depth of penetration (DOP). It is found that the DOP scales slightly non-linearly with the impact velocity. The core velocity during the penetration process is also slightly nonlinear. The deceleration during penetration is almost a linear function of the penetration velocity and it is higher for higher penetration velocities.

Keywords: Inclined impact, Polycarbonate, Ricochet , Trajectory, Simulation

(*) Corresponding author: dorogoy@technion.ac.il

1. Introduction

Transparent polycarbonate (PC) is well known for its high ballistic resistance to penetration and perforation, and is widely used in impact-resistant applications. Hence numerous investigations have been carried out to characterize its static and dynamic flow and failure properties (e.g. Ravi-Chandar [1], Rittel *et al.* [2-6] and Sarva *et al.* [7]). Concerning its penetration behavior, quasi-static deep penetration tests using circular cylindrical hardened steel punches were conducted by Wright *et al.* [8]. These authors noticed that the plastic zone diameter equals 3.5 times the punch diameter, and that the refractive index of PC changes markedly at yield. They also showed a damaged zone containing small cracks fully contained within the plastic zone which extends over 1.4 times the punch diameter. The resistance of thin PC plates (2, 5 and 12mm) to impact by round and cylindrical projectiles was investigated experimentally by Wright et al. [9] who identified five main types of plate behavior: elastic dishing, petalling, deep penetration, cone cracking and plugging. Inclined impact on thin PC plates (less than 6.4 mm thick) was also investigated by Li and Goldsmith [10], who noticed that the resulting perforation hole exhibits a much smaller diameter than the projectile, indicating a substantial capability for recovery. The ballistic resistance of clamped thin PC plates to single [11] and multiple ballistic impacts [12] was investigated as well. It was concluded that reinforcements should be provided near the clamped edges.

Following Rosenberg *et al.* [13], a study was conducted on inclined impact of polymethylmethacrylate (PMMA) thick plates [14] in which the combined effects of brittle (spalling) and ductile failure mechanism were included. Such an investigation has not yet been carried out on thick polycarbonate plates. Hence, this investigation addresses the inclined ballistic impact of thick polycarbonate plates by a 7.62 mm armor piercing projectile under the combined effects of tensile (brittle) and ductile failure mechanisms. The investigation is done by performing ballistic experiments aimed at validating the numerical simulations, which can further be used for predictive purposes.

The paper is organized as follows: First the experimental results are presented, followed by the numerical model and its results. The latter are compared to the experimental results and discussed. A study of the maximum depth of penetration in normal impact is

then conducted. The main results of this study are then summarized, followed by a concluding section.

2. Experiments

2.1 Experimental setup

The experiments were performed in the Ballistics laboratory at RAFAEL using 7.62mm armor piercing projectiles. The core of this projectile weighs 4.01 grams and the typical muzzle velocity is ~750 m/s. The targets were positioned some 7m from the gun, at various angles of inclination 0^{o}, 20^{o}, 25^{o}, 30^{o}, 40^{o} , 60^{o} and 80^{o} (relative to the projectile line of flight). The targets were made of 50mm thick square plates of lateral dimensions $250\times80\ mm^{2}$. One experiment was conducted using 60^{o} inclination and three layered (but not attached) plates to investigate the depth of penetration. The thickness of the plates in this specific experiment was 40 mm. Three 150 kV flash X ray tubes were used to follow the penetration of the projectile. Three pictures were recorded. The first was taken just before impact and the following two other pictures covered the time interval of 90 - 150 μs thereafter. The projectile's trajectory within the targets was recorded and the trajectory length within the plate was measured after the test.

2.2 Experimental results

For a single 50 mm thick plate, bullet ricochet was observed only for a 20^{o} and 25^{o} inclination, while perforation occurred for all the other angles. For a stack of three 40 mm thickness plates, the projectile came to a halt within the third plate. In all the tests it was observed that: 1) The core of the projectile penetrated and perforated the plates but came out undamaged. 2) The copper jacket of the projectile was destroyed during early penetration, and its remains could be seen along the projectile trajectory within the plates. The trajectories shapes will be shown and further discussed in the numerical results section later on.

2.2.1 Common characteristics of the trajectories

Fig. 1 shows a section through the trajectory in a perforated 50 mm thick plate impacted at 80^{o} inclination. Three distinct regions can be observed along the trajectory: a. Entrance, b. Internal propagation, and c. Exit.

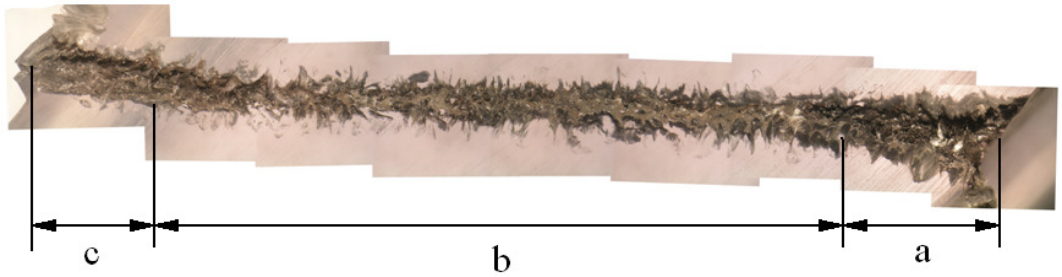

a.

b.

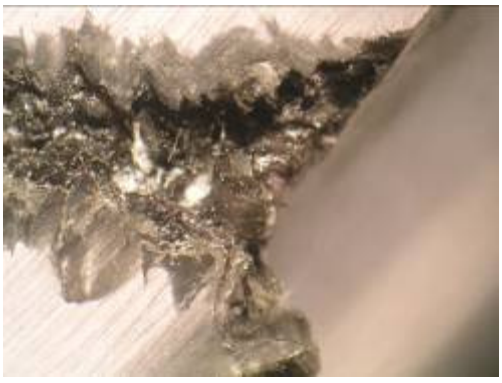

c.

Figure 1: A section through a typical trajectory within a perforated 50 mm thick polycarponate plate struck by a 7.62mm armor piercing projectile. a. The whole section through the trajectory showing: a. Entrance, b. Internal propagation, and c. Exit. . b. The exit region. c. The entrance region. Note the extensive damage along the trajectory, essentially comprised of microcracks and breakage.

The entrance and exit are characterized by a larger cavity diameter and a slight change of direction. Inside the plate, the cavity is straight and narrow. Two different damage zones are observed in Fig. 1 along the trajectory path: a. Cavity. b. A cylindrical cracked zone around the cavity.

Figs. 2a and 2b show that the cavity and the cylindrical cracked zone are surrounded by another cylindrical zone which has changed its refractive index. This change is due to plastic deformation and probably significant evolution of heat that ocurred during the perforation, as also been reported by Wright *et al.* [8]. This plastic zone has a typical diameter of ~9-10 mm. The core of the projectile is not damaged during perforation as can be seen in Fig. 2b.

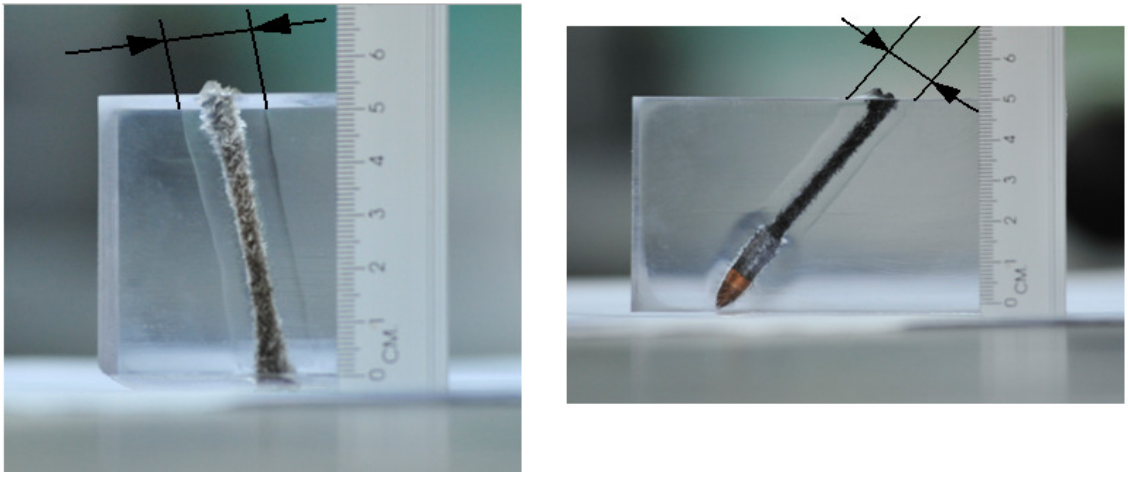

a. b.

Figure 2: Trajectory within thick polycarponate plates. a. Perforation at 80^{o} showing the affected plastic zone around the cavity, marked by arrows. b. A 60^{o} penetration showing the affected plastic zone around the core and the cavity. Note the change of refractive index in the plastic zone, as well as the significant recovery of the cavity along the trajectory, as evidenced from its smaller diameter compared to the core dimension.

The significant recovery of the PC is also visible in Fig. 2b. The core diameter is 6.05 mm while the cavity diameter is 3-4 mm.

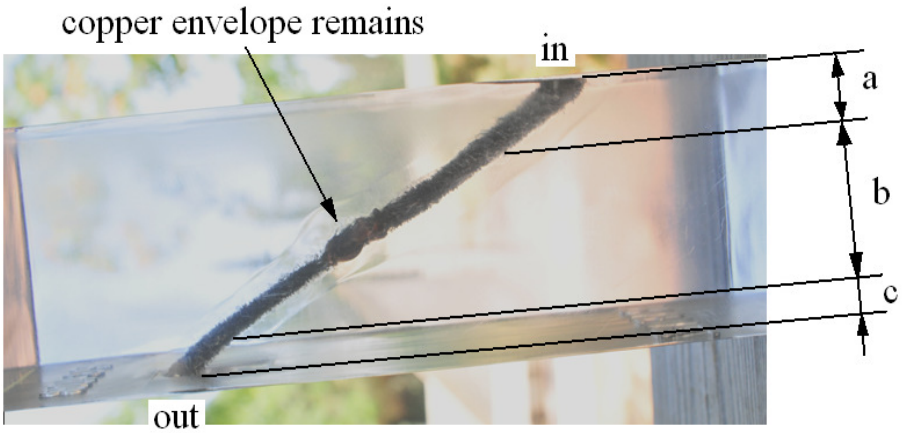

a.

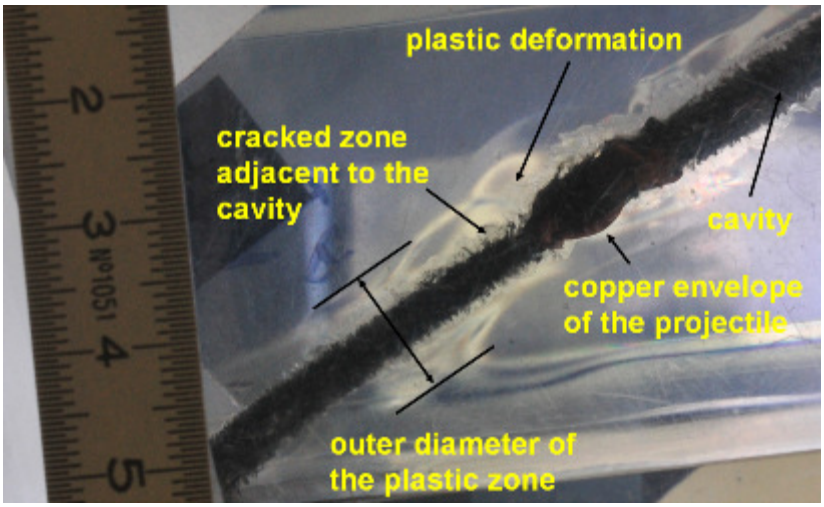

b.

Figure 3: The trajectory within PC plate which was perforated by a 30^{o} impact. a. The three distict regions: 1. Entrance (a), 2. Internal propagation (b), and 3. Exit (c). b. A detailed view of a trajectory close to the copper remains showing three distinct damage zones: cavity, plastic zone and a cracked zone adjacent to the cavity and fully confined within the plastic zone.

Fig. 3 shows another polished section of a PC plate, which was perforated by a 30^{o} impact. Three distinct regions can be observed along the trajectory(Fig. 3a): a. Entrance,

b. Internal propagation, and c. Exit. The entrance is characterized by a large diameter cavity and a slight change of direction. Inside the plate, the cavity is straight and narrow, and at the exit it remains narrow but changes its direction towards the free surface. The remains of the copper jacket can be seen along the trajectory. A detailed picture of a trajectory (using polarizers) is shown in Fig. 3b. Three distict damage zones can be observed: cavity, cracked zone and plasticaly deformed zone. The cavity has a varying diameter which is smaller than that of the projectile's core. The diameter of the cavity is ~3.8 mm while the diameter of the projectile core is 6.05 mm. This fact indicates again that a significant recovery of the PC is occurring.

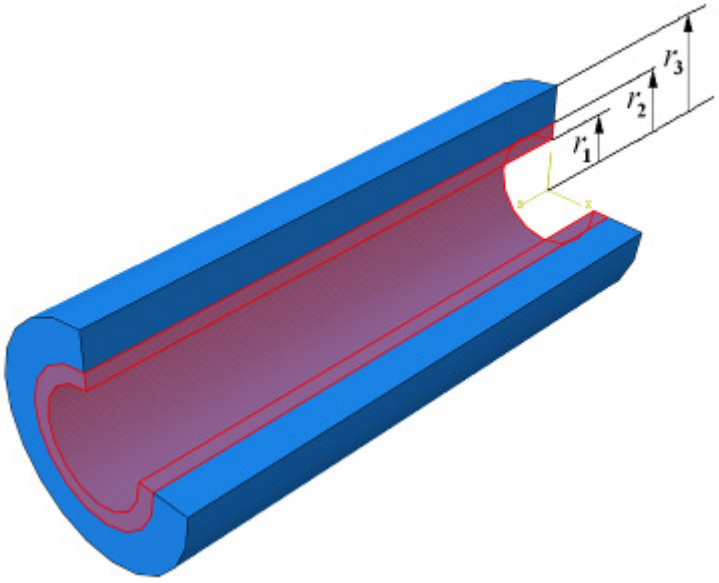

Figure 4: Schematic structure of the damaged zone of a trajectory showing the cavity (r_1) radius , the cracked region radius (r_2) and the plastic zone radius (r_3).

A schematic structure of the trajectory regions of damage is shown in Fig. 4. The plastic zone is surrounding the cavity and the cracked zone and its radius $r_3 \approx 4.0-4.5\ mm$ The cracked zone is fully confined within the plastic zone and its thickness is $\Delta \equiv r_2 - r_1 \approx 1\ mm$. The cavity is narrow $r_1 \approx 1.5-2\ mm$.

2.2.2 X ray pictures of the perforation process

Typical X-ray pictures of a projectile penetrating the polycarbonate plate at 30^{o} inclination are shown in Fig. 5. The first picture, (1), was taken when the projectile just comes in contact with the plate. The second picture, (2), was taken after 90 μs and shows that the projectile has just completed penetration of the plate. The third picture (3) was taken 230 μs after the first picture and 140 μs from the second one, and shows that the projectile is still well within the plate. The "long" dwelling (t > 230 μs) of the projectile within the plate indicates that the PC is significantly slowing down the projectile velocity.

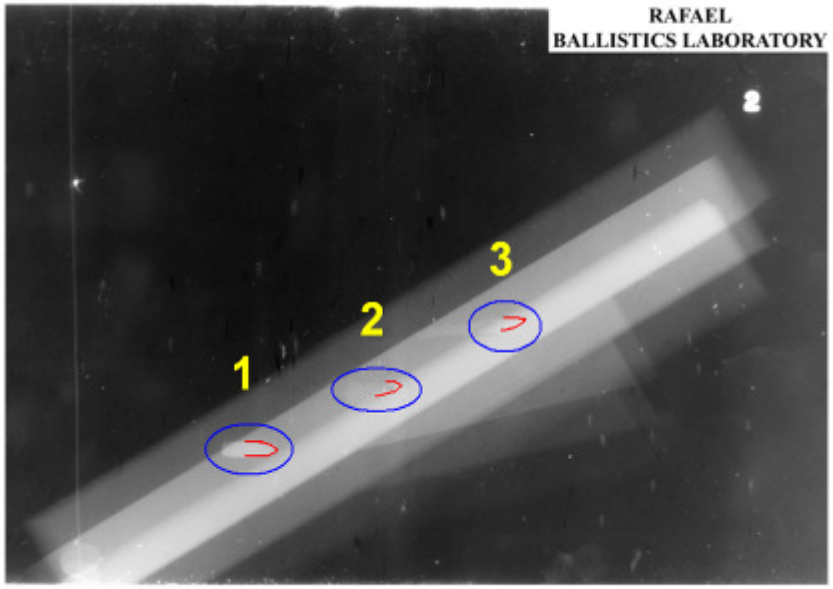

Figure 5: 7.62 mm projectile impacting at 750 m/s. Three X ray pictures taken at 90 μs and 140 μs intervals of penetration into a 50 mm thick single polycarbonate plate

3. Numerical simulation

The idea is to develop an ultimately predictive model to help in design, minimize the number of ballistic tests, also provide insight into the penetration process. The type of analysis, geometry, material properties, failure criteria and mesh are detailed in the sequel. A numerical convergence to the experimental results for a specific mesh size is first shown, followed by more examples of one and three plates. A prediction for the depth of penetration is given as well with a comparison with ballistic test.

3.1 Analysis

A 3D transient adiabatic analysis was conducted with the commercial FE code Abaqus/CAE 6.9-EF1 [15]. The hydrodynamic continuum equations are derived from application of the conservation laws of mass, momentum, and energy. An equation of state provides the relationship between pressure, density, and internal energy. An elastic-plastic Mises plasticity model is used for constitutive relations. An overview of the theory of hydrocodes can be found in [16]. The constitutive behavior of polycarbonate was represented using a hydrodynamic material model in which the material's volumetric strength is determined by a linear Mie-Grüneisen equations of state[17], while the deviatoric behavior is of the isotropic elastic- plastic Mises-type. Two failure criteria [17]: (1) tensile failure (2) ductile damage with damage evolution, were used. These failure criteria will be detailed in section 3.4.

The general contact algorithm of Abaqus [15] was used with element-based surfaces which can adapt to the exposed surfaces of the current non-failed elements. All the surfaces that may become exposed during the analysis, including faces that are originally in the interior of body were included in the contact model. This means that we included all the elements of the plate and the projectile in the contact domain since the projectile trajectory is not known *a priori*. We chose the software parameters so that contact nodes

still take part in the contact calculations even after all of the surrounding elements have failed. These nodes act as free-floating point masses that can experience contact with the active contact faces. A frictionless contact was assumed to exist between all contacting faces (interior and exterior).

3.2 Geometry

The impact of a 7.62 mm projectile traveling at 750 m/s at inclination angles of 0^o - 80^o on a polycarbonate plate was modeled. The assembled geometry for a 20^o impact is shown in Fig. 6a. Because of symmetry only half of the geometry was modeled. The projectile is assumed to be made of a hard steel core embedded in a copper envelope as seen in Fig. 6b.The dimensions of the hard steel core are shown in Fig. 6c.

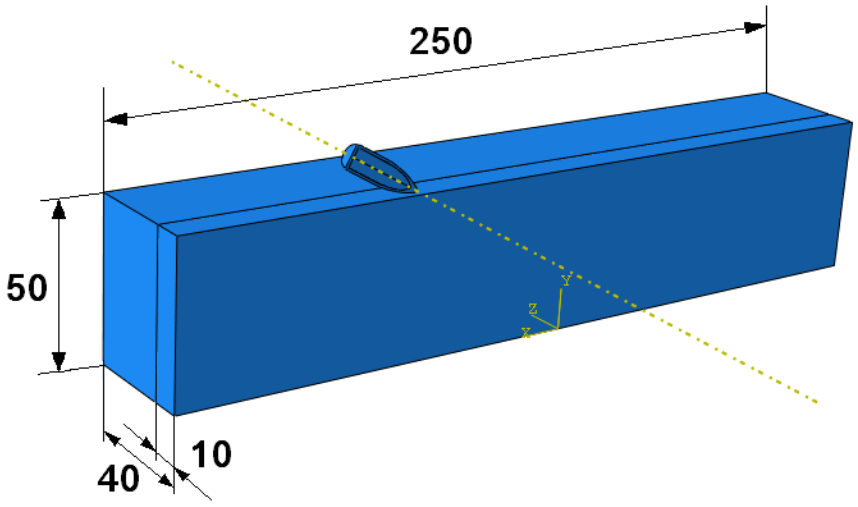

a.

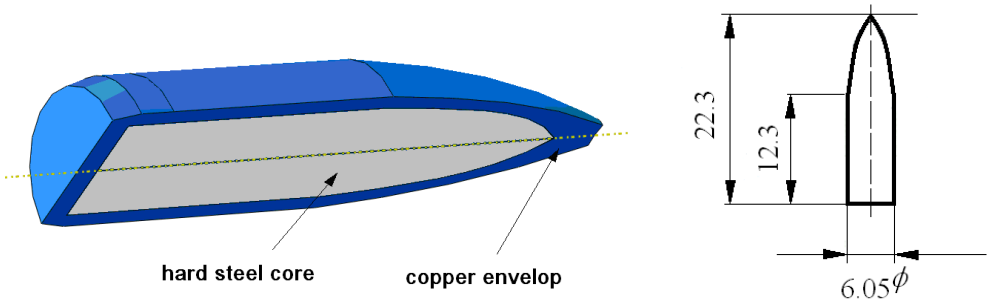

b. c.

Figure 6: a. The half model: the inclined projectile with the polycarbonate plate. b. the half modeled projectile. c. The steel core dimensions .

The dimensions of the polycarbonate plate model are 250 mm long, 50 mm thick and 40 mm wide. The projectile weighs a total of 7.42 gr, out of which the hard steel core weighs 4.04 gr.

3.3 Material properties

The *copper jacket* was modeled as an elastic-plastic material with ductile damage and damage evolution ([17]). The *steel core* was assumed to be elastic that does not fail or erode. Finally, a hydrodynamic material model in which the material's volumetric strength is determined by an equation of state was used for the *polycarbonate plate*, namely the Mie-Gruneisen equation of state (EOS) with application of linear U_s-U_p Hugoniot. U_s is the linear shock wave and U_p is the particle speed. This model can be applied to materials which also have isotropic elastic or viscous deviatoric behavior. It is used with a Mises plasticity model. More details can be found in *Abaqus Analysis User's Manual in* chapter: 21.2.1 Equation of state [17]. The hydrodynamic material data for the polycarbonate was taken from [18] who used the AUTODYN^{TM} material libraries. . The elastic properties of the materials are summarized in table 1 while the phsical properties in table 2. The hydrodynamic data for the polycarbonate are given in table 3. The isotropic elastic linear shear behavior was given a value of 803 MPa for T=0 ^{o}C and a value of 80.3 MPa for temperature elevation of T=200ºC, based on [19]. The strain-rate and temperature dependence of the plastic behavior is shown in Fig. 7. The strain rate dependence is based on our experimental results with cylindrical specimens [20], and

uses a linear extrapolation for plastic strains up to 1. The strain stress curve for strain rates exceeding 8000 1/s was assumed to be identical to that of 8000 1/s. This extrapolation is used due to the lack of experimental data. It was assumed that at T=100^{o}C for all strain rates, the PC softens and the yield stress is half of the quasi static one, while at T=200^{o}C it drops almost to zero, and the material flows freely [19].

Table 1: Elastic properties of the materials modeled in the simulation

material	E [GPa]	ν
copper	115	0.358
steel	210	0.300
polycarbonate	2.2	0.370

Table 2: Physical properties of the materials modeled in the simulation

material	ρ [Kg/m^3]	Specific Heat $c_p \left[\frac{\text{J}}{\text{Kg K}^o}\right]$	Inelastic Heat Fraction
copper	8940	-	-
steel	7800	-	-
polycarbonate	1200	1300	1

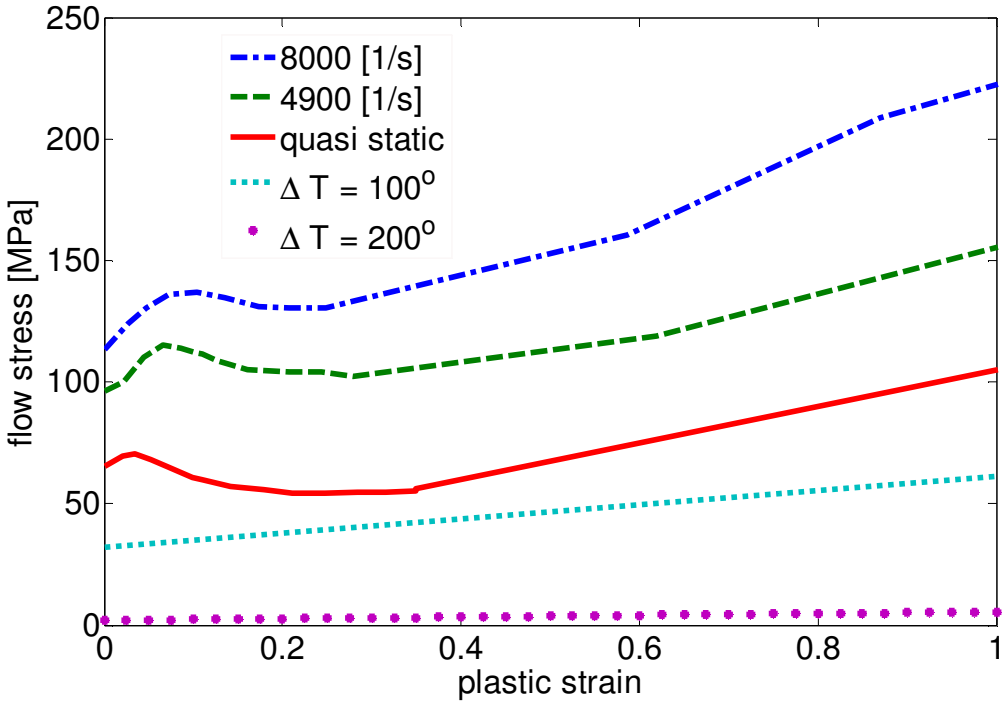

Figure 7: Plastic properties of polycarbonate which were used in the numerical analyses.

Table 3: Hydrodynamic data for polycarbonate (reference [18])

Reference density ρ_0 [kg/m3]	1910
Bulk sound speed c_0 [m/s]	1933
Slope s in Us versus Up diagram	2.65
Gruneisen coefficient Γ_0	0.61

3.4 Failure criteria and data

Two failure criteria were used for the polycarbonate: 1) tensile failure, 2) ductile damage with damage evolution. The same two criteria were used in Dorogoy *et al.* [14].

3.4.1 Tensile failure [17]

The "tensile failure" uses the hydrostatic pressure as a measure of the failure stress to model dynamic spall, or a pressure cutoff. Failure occurs when the pressure $\sigma_{cutoff} = \frac{\sigma_{ii}}{3}$, becomes more tensile than a (user-specified) hydrostatic cutoff stress, $\frac{\sigma_{ii}}{3} > \sigma^{*}_{cutoff}$. This criterion is suitable for high-strain-rate deformation and offers a number of choices to model failure, including removal of elements from the mesh. It can also be used in conjunction with other failure criteria.

3.4.2 Ductile failure[17]

The "ductile failure" criterion is used to predict the onset of damage due to nucleation, growth and coalescence of voids. The model assumes that the equivalent plastic strain at the onset of damage $\bar{\varepsilon}^{pl}_{D}$ is a function of the stress triaxiality (η) and plastic strain rate ($\dot{\bar{\varepsilon}}^{pl}$), $\bar{\varepsilon}^{pl}_{D}\left(\eta\ ,\ \dot{\bar{\varepsilon}}^{pl}\right)$. The stress triaxiality is given by $\eta = -p/q$, where p is the hydrostatic pressure, q is the Mises equivalent stress, and $\dot{\bar{\varepsilon}}^{pl}$ is the equivalent plastic strain rate. The damage variable, $\omega_D = \int \frac{d\bar{\varepsilon}^{pl}}{\bar{\varepsilon}^{pl}_{D}\left(\eta, \dot{\bar{\varepsilon}}^{pl}\right)}$, increases monotonically with plastic deformation. At each increment during the analysis the incremental growth in ω_D is computed as $\Delta\omega_D = \frac{\Delta\bar{\varepsilon}^{pl}}{\bar{\varepsilon}^{pl}_{D}\left(\eta, \dot{\bar{\varepsilon}}^{pl}\right)} \geq 0$. The criterion for damage initiation is met when $\omega_D = 1$. The way the material behaves after initiation until final failure is defined by "damage evolution", as discussed next.

3.4.3 Damage evolution [17]

Damage evolution is specified in terms of a mesh independent constant such as an equivalent plastic displacement $\bar{u}^{p}_{f}$ at the point of failure. The criterion assumes that

damage is characterized by a linear progressive degradation of the material stiffness, leading to final failure. Once the damage initiation criterion has been reached, the effective plastic displacement, $\bar{u}^{pl}$, is defined with the evolution equation $\dot{\bar{u}}^{pl} = L\dot{\bar{\varepsilon}}^{pl}$, where L is the characteristic length of the element. The damage variable D increases according to $\dot{D} = \frac{\dot{\bar{u}}^{pl}}{\bar{u}_f^{pl}}$. This definition ensures that when the effective plastic displacement reaches the value $\bar{u}^{pl} = \bar{u}_f^{pl}$, the material stiffness will be fully degraded as D = 1. At any given time during the analysis, the stress tensor in the material is given by the scalar damage equation, $\sigma = (1-D)\bar{\sigma}$, where D is the overall damage variable and σ is the effective stress tensor computed in the current increment. The tensor $\bar{\sigma}$ represents the stresses that would exist in the material in the absence of damage. By default, an element is removed from the mesh if all of the section points at any one integration location have lost their load-carrying capacity.

3.4.4 Data for failure criteria

The tensile failure value was set to 160 MPa. The damage initiation values are summarized in table 4. These values are based on experimental results obtained by torsional split Hopkinson bar [21] in which fracture ocured at shear strain $1.5 \le \gamma \le 2.0$. The linear displacement damage evolution value used is 80 [μm], which was also used for PMMA in [14].

The failure criterion "ductile damage with damage evolution" was also used for the copper enveloppe, A constant value of plastic strain of 0.4 was used for all triaxialities, temperatures and strain-rates with a zero linear displacement damage evolution.

These values were selected because they were found to yield a satisfactory reproduction of the experimental trajectories, including the ricochet phenomenon for angles of inclination smaller than 20^{o} .

Table 4: Damage initiation values and damage evolution for polycarbonate.

Strain rate [1/s]	polycarbonate
Quasi static	1.0
4900	0.85
8000	0.85
80000	0.60
Damage evolution [μm]	80

3.5 Mesh

The results are mesh dependent, as would be expected from element deletion considerations. Hence a constant mesh size was used through out this work in the regions were the projectile trajectory develops. The constant size of the elements in all 3 directions was chosen to be 1.25 mm. This size was chosen based on convergence of the numerical results to the experimental ones. This convergence will be shown in the sequel. A typical mesh which is shown in figure 8a consist of 86213 elements. 82665 linear hexahedral elements of type C3D8R on the plate and 3548 linear tetrahedral elements of

type C3D4 on the core and its copper envelope. 38577 out of the 82665 were assigned to the 10 mm width of constant mesh zone shown in Fig. 6 and visible on Fig 8b.

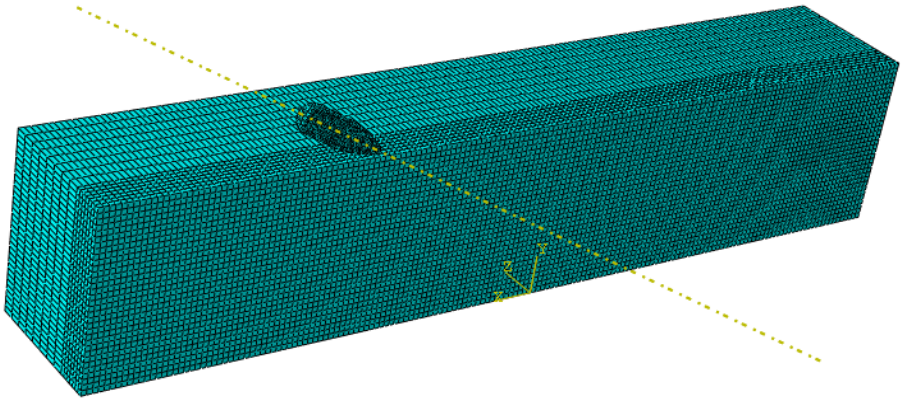

a.

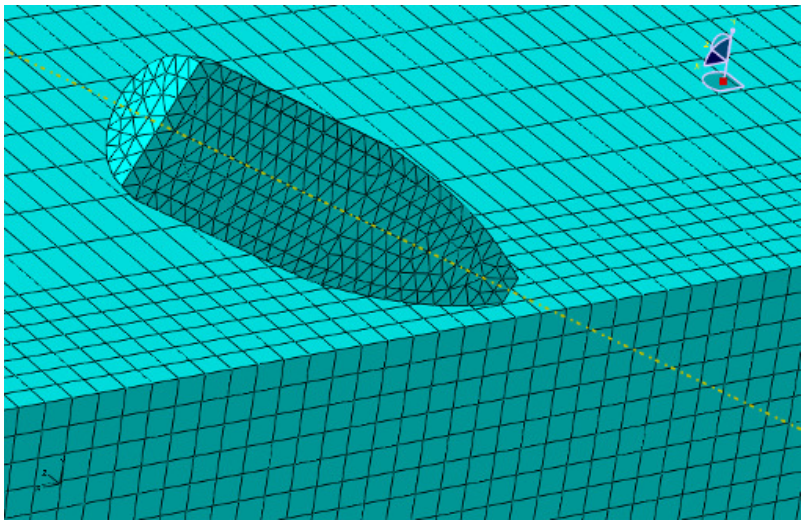

b.

Figure 8: A typical mesh used for calculations. a. The whole mesh. b. Detailed view near impact location showing the constant mesh size..

3.6 Numerical Results

The numerical results are compared to the experimental resuts obtained for inclined impact of 1 and 3 plates in order to assess their reliability. Next a numerical investigation of the depth of penetration (DOP) is presented.

3.6.1 Mesh size convergance

Since the numerical results are mesh dependant a constant mesh size was adopted. The material parameters detailed in sections 3.3-3.4 and 4 different constant mesh size of 1.75, 1.5, 1.25 and 1.0 mm were used to simulate the impact with 750 m/s at angle of inclination 30^{o} . The resulting numerical trajectories are shown in Fig. 9a-9d . The experimental trajectory is shown in Fig. 3a and Fig. 5.

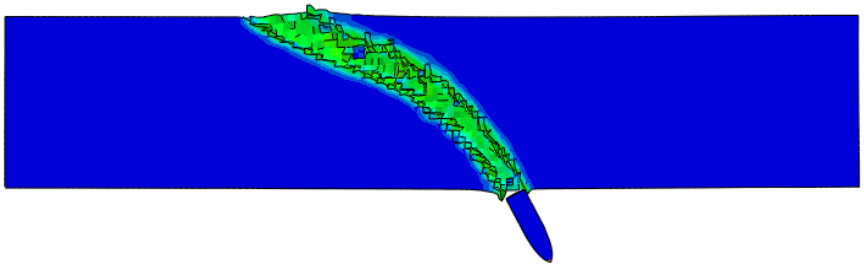

a.

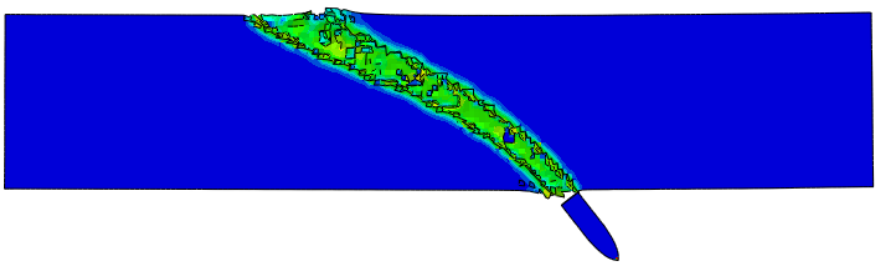

b.

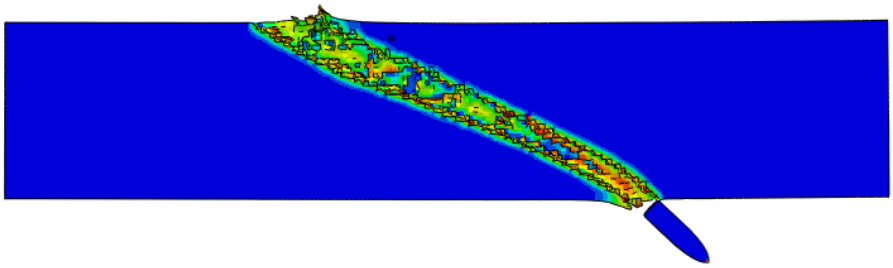

c.

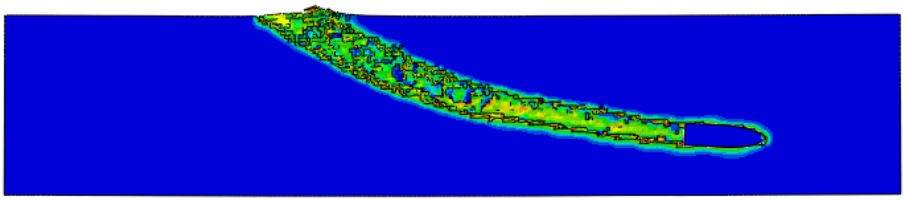

d.

Figure 9: Numerical trajectories due to inclined impact of 750 m/s at 30^{o} due to to different mesh sizes. a. mesh size of 1.75 mm. b. Mesh size of 1.5 mm. c. Mesh size of 1.25 mm. d. Mesh size of 1.00 mm.

The mesh size of 1.75 results in a short trajectory. The mesh size of 1.5 results with a similar trajectory to the experimental one but with a very long time of perforation ~500 μs, which is longer than what is observed in figure 5. The mesh size of 1.25 results with a similar trajectory to the experimental one but with a perforation time of 420 μs which is close to what can be estimated from Fig. 5. For mesh size of 1 mm the projectile does not perforate the plate. Based on these observations a constant mesh size of 1.25 mm was used throuout this work for the polycarbonate plates.

3.6.2 Results for 30^{o} inclination

The numerical trajectories shown in Figs 10a and 10b are showing the projectile position after 90 μs and 230 μs. These trajectories were obtained using the 1.25 mm constant mesh size. These trajectories can be compared to positions 2 and 3 in Fig. 5 which show the X ray pictures at 90 μs and 230 μs. A satisfactory qualitative agreement can be observed which indicate that the numerical speed of the projectile within the PC plate is close to the experimental one.

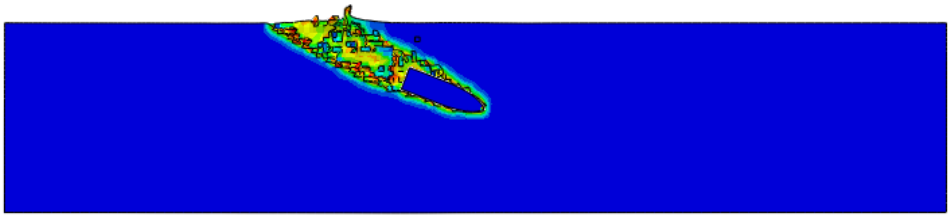

a.

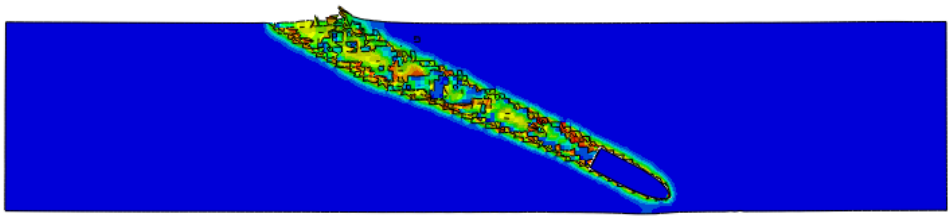

b.

Figure 10: Trajectories of inclined impact at 30°. a. After 90 μs. b. After 230 μs.

The numerical trajectory and the experimental trajectory are compared in figure 11. Points (x,y) were downloaded from the numerical analysis and from a picture of the experimenatal results and are plotted in figure 11. The numerical data was smoothed. A good agreement can be observed for the main characteristics of the trajectory. The three

regions of the trajectory namely: Entrance (a), propagation (b) and exit (c) are observed. The cavity diameter in the entrance (a) and exit(c) is larger than along the the propagaton region (b).

The difference in the horizontal length is ~12 mm out of 125 mm which is less than 10%.

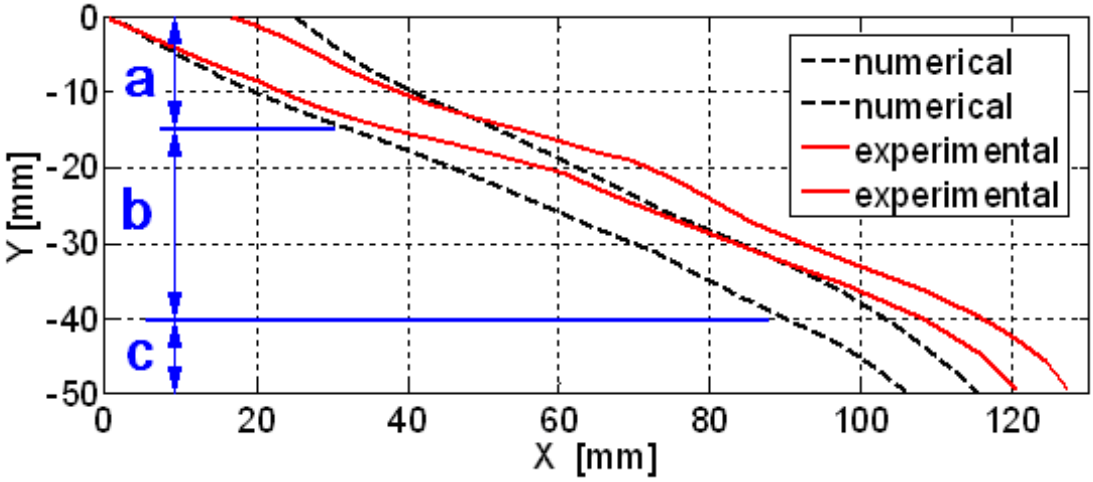

Figure 11: Comparison between numerical and experimental trajectories for 30^{o} impact.

3.6.3 Effect of failure criteria

The effect of each failure criteria on the trajectory was checked by applying each of them separately. The trajectory which is obtained numerically by application of the "ductile failure with damage evolution" is shown in Fig. 12a, and that obtained by application of the "tensile failure" criterion is shown in Fig. 12b. It can be observed that separate application of each of the failure criteria alone does not result in total perforation of the plate. It can also be observed that the main contribution to the trajectory is done by the "ductile failure with damage evolution" criterion. The simultaneous usage of both criteria

result in the trajectory shown in Figs. 3, 9c and 11, which faithfully reproduces the observed perforation.

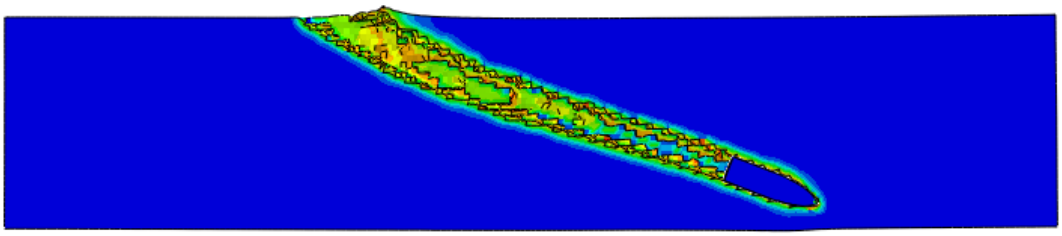

a.

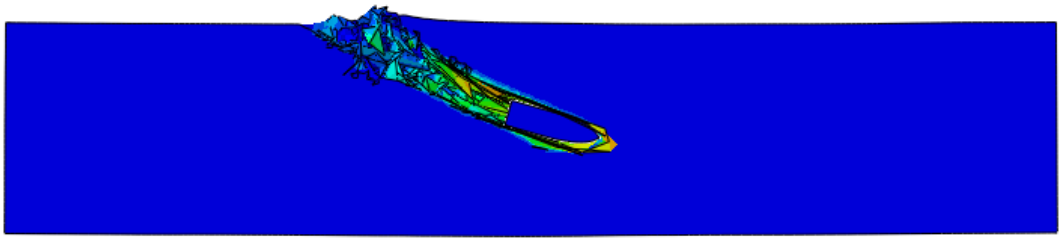

b.

Figure 12: Effect of failure criteria on the trajectory for 30^{o} impact. a. Using only ductile failure with damage evolution. b. Using only tensile failure.

3.6.4 Inclined impact of one plate

The numerically obtained trajectories for angles of inclinations: $0^{\circ} \le \theta \le 90^{\circ}$ can be divided into three regions : 1) $0^{\circ} \le \theta \le 17.5^{\circ}$ ricochet , 2) $17.5^{\circ} < \theta < 30^{\circ}$ penetration and arrest , 3) $\theta \ge 30^{\circ}$ full perforation.

These regions are compared to the experimental ones in table 5. The numerical and experimental results show a very good agreement regarding the angle at which full perforation of the plate occurs (30^o). Experimentally the highest angle at which ricochet occurs was found to be 25^o. Numerically, the highest angle of inclination at which ricochet occurred was calculated to be 17.5^o. For $17.5^\circ < \theta < 30^\circ$ the projectile penetrated the plate and did not perforate it.

The numerically obtained trajectories at $\theta = 12.5^\circ, 17.5^\circ, 40^\circ$ and 80° inclination are shown in Fig. 13 a-d respectively. The experimental length (top view) of the trajectory at 20^o inclination is 70 mm and it is very similar to the numerical trajectory obtained at 12.5^o inclination and shown in Fig. 13a. The numerical trajectory at 17.5^o shown in Fig. 13b is longer, which might indicate that the real material has a higher "resistance" to penetration at $\theta < 30^\circ$ than the simulated one. Figure 13c show the trajectory due to 40^o inclination with a horizontal length of 84.5 mm, which agrees with the experimental trajectory of 83 mm long. The trajectory due to 80^o inclination shown in Fig. 13d and it agrees again with the experimental trajectory of Fig. 2a.

Table 5: Numerical - experimental comparison for trajectory type

	numerical	experimental
ricochet	$0^\circ \le \theta \le 17.5^\circ$	$0^\circ \le \theta \le 25^\circ$
penetration	$17.5^\circ \le \theta < 30^\circ$	-
perforation	$\theta \ge 30^\circ$	$\theta \ge 30^\circ$

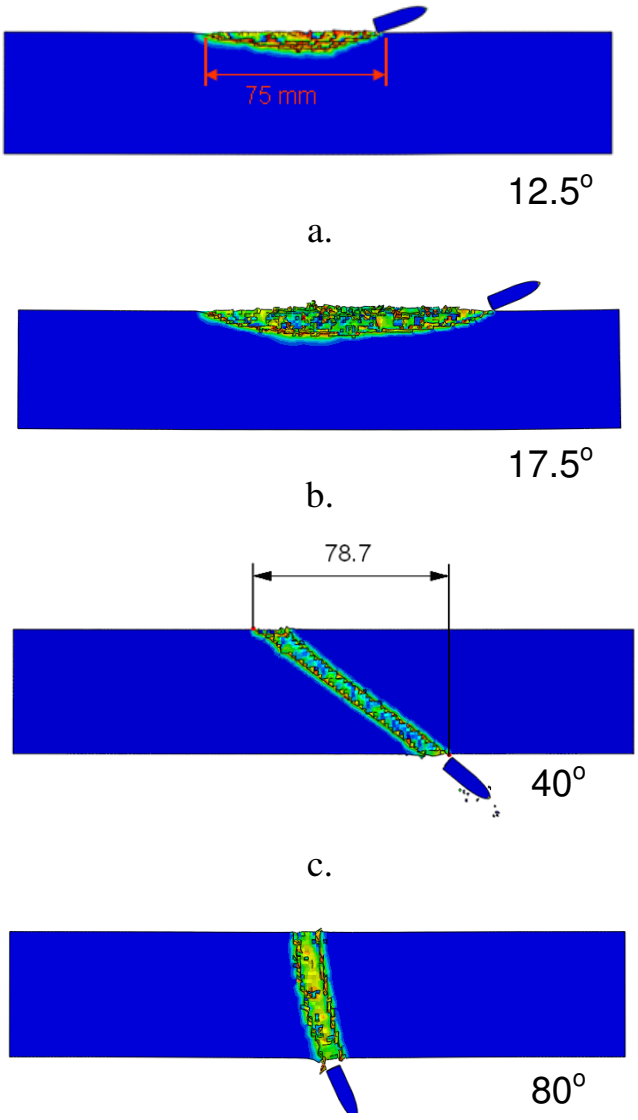

Figure 13: trajectories of an armor piercing projectile impacting at 750 m/s. a. Numerical ricochet trajectory for 12.5° inclination. b. Numerical ricochet trajectory for 17.5° inclination. c. Numerical trajectory for 40° inclination. d. Numerical trajectory for 80° inclination.

3.6.5 Inclined impact on three layered plates

Three layered polycarbonate plates with lateral dimensions of 300×120 *mm* and thickness of 40 mm were experimentally impacted with the same 7.62 mm armor piercing projectile at 740 m/s and 60^{o} inclination. This setup was simulated numerically and the calculated trajectory is shown in Fig. 14a. The yellow line in Fig. 14a represents schematically the experimental trajectory. A good agreement is observed.

Bottom views of the experimental trajectories in each plate are shown in Fig. 14b-d. There is a good agreement between the numerical and experimental results regarding the main features of the trajectory. The numerical simulation predicts that the core will penetrate the third plate and stop within it, similar to the experimental observation. The numerical simulation predicts that the trajectory in the second plate will be longer than that in the first plate. This fact is also seen in the experimental resuls. The deflection of the core in the second plate is probably due to build up of pressure underneath the core.

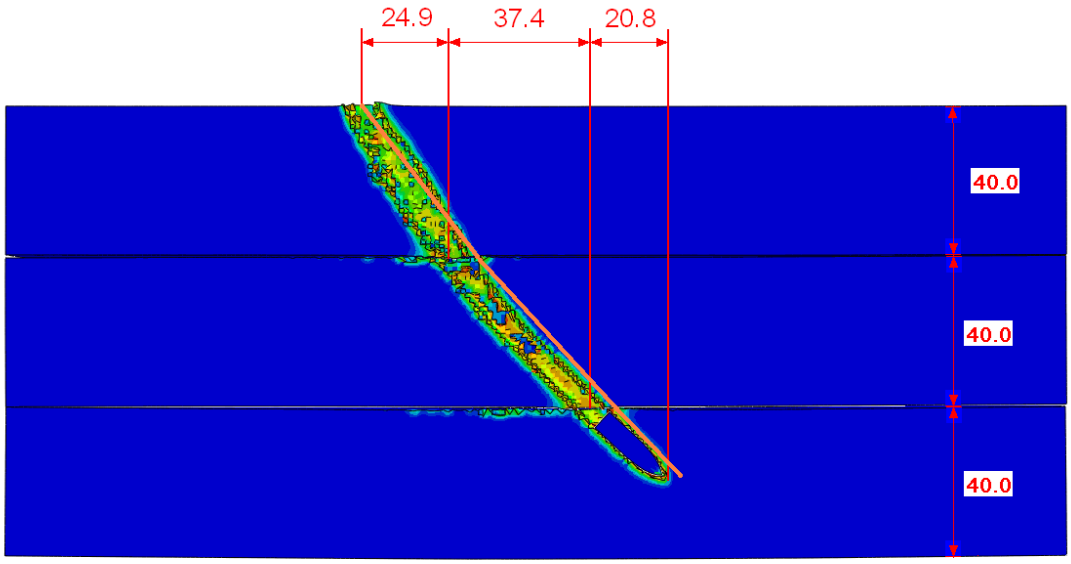

a

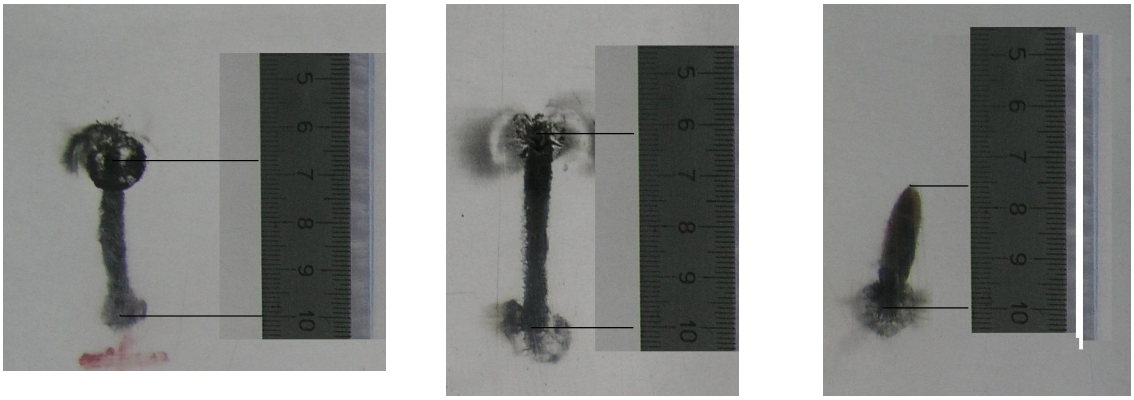

b. c. d.

Figure 14: Numerical and experimental trajectory within 3 stucked plates impacted with 740 m/s at 60°. a. A cut view of the numerical and experimental trajectory. b.Bottom view of the upper plate trajectory. c. A Bottom view of the middle plate trajectory. d. Bottom view of the third plate trajectory showing the stopped core of the armour piercing projectile

3.7 The maximum depth of penetration (DOP)

Since a fairly satisfactory agreement was obtained between the experimental results and the numerical simulations, the effect of the velocity on the depth of penetration was studied numerically. Five numerical analyses at five different impact velocities: 250, 400, 500, 600 and 750 m/s were performed. The PC plate is 250 mm long, 200 mm thick and 80 mm wide. Because of symmetry, only one half of the physical domain is modeled. The modeled deformed geometry is shown in Fig. 15 for penetration of a steel projectile impacting the plate at 750 m/s. The results of the corresponding DOP are listed in Table 6 and plotted in Fig. 16. The dots represent the numerical results. and the lines represent the DOP quadratic approximation: $DOP(V_i) = aV_i^2 + bV_i$ [mm], a = 0.000172 , b = 0.06304.

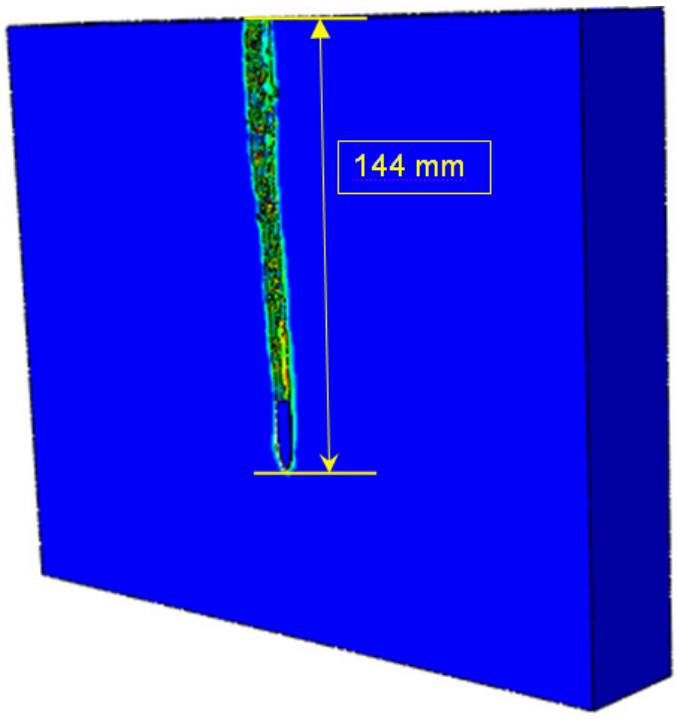

Figure 15: The modeled plate showing the DOP of 7.62 mm armor piercing projectile impacting a thick PC plate at 750 m/s.

Table 6: DOP for impact velocity $150 \leq V_i \leq 750$ m/s.

V_{impact} $[m/s]$	DOP [mm]
250	25.9
400	51.9
500	75.6
600	100.6
750	143.5

It can be noted that the DOP scales almost linearly with the impact velocity higher than 200 m/s. The velocity of the core during normal penetration for impact velocities of 250 <Vi<750 [m/s] are shown in Fig. 17a. The velocities during penetration are slightly non linearily in time. For each impact velocity the deceleration was calculated and plotted versus the penetration velocity in Fig. 17b. It can be observed that for impact velocities 750, 600,, 500 and 400 m/s, all the curves coincide. The discrepancy of impact velocity 250 m/s is probably due to numerical errors because of the shorter DOP and time to a halt. It can be observed that the deceleration is almost linear with the penetration velocity. It is higher at higher velocities, meaning that the material has higher resistance to penetration at higher velocity.

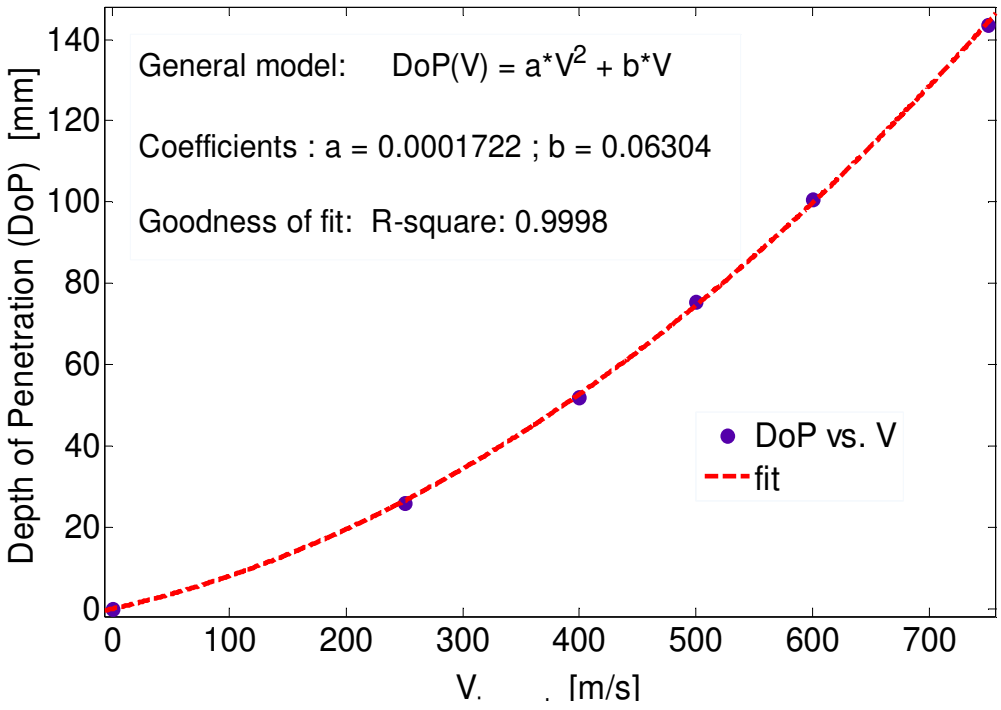

Figure 16 :The DOP vs. impact velocity for normal penetration in PC

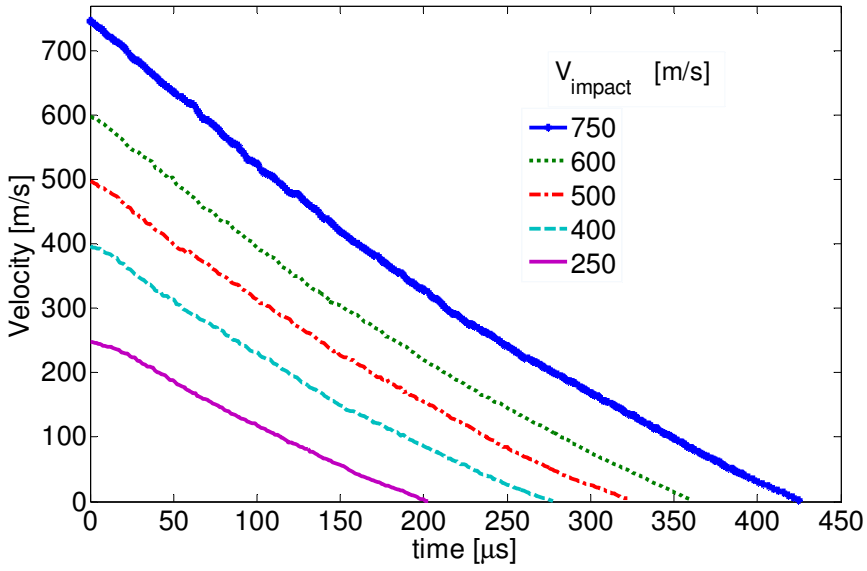

a.

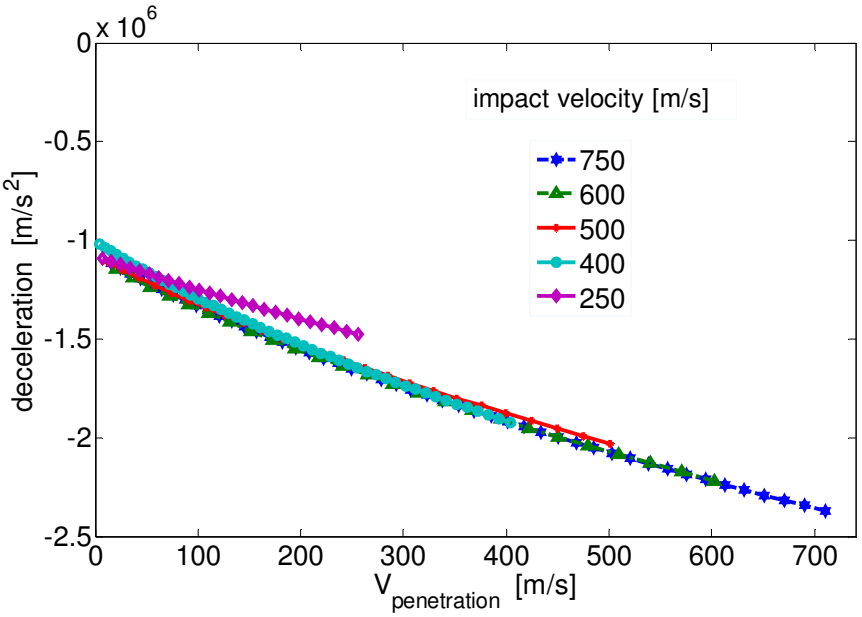

b.

Figure 17 : The velocity and deceleration of the core during normal penetration for impact velocities 250 <Vi<750 [m/s]. a. Velocity versus time. b. Deceleration versus penetration velocity.

3.7.1 Experimental verification of the DOP

A cylindrical block of polycarbonate having a diameter of 127 mm and height 243 mm was normally impacted at a velocity of 754 m/s. The block is seen in Fig 18a. The cylinder was machined, and the trajectory is shown in Fig. 18b. The depth of penetration is 138 mm. The numerical calculated DOP, shown in Fig. 15, is 144 mm which is only 4% difference from the experimental result. This test verifes the numerical results and the predictive capability of the numerical model.

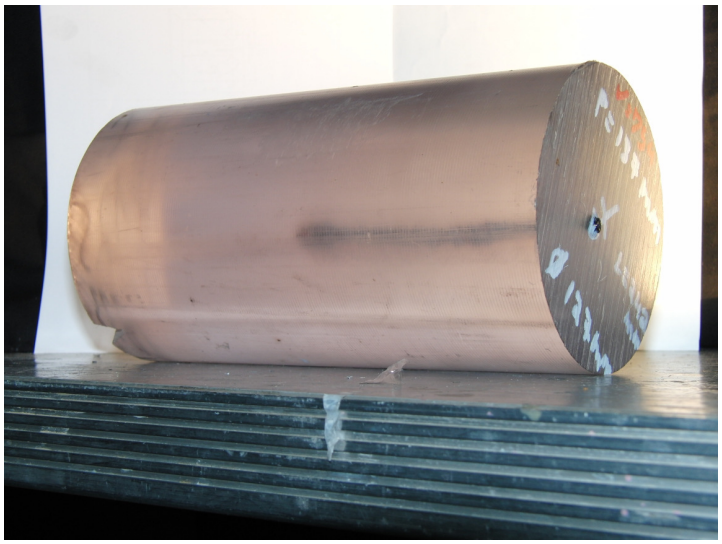

a.

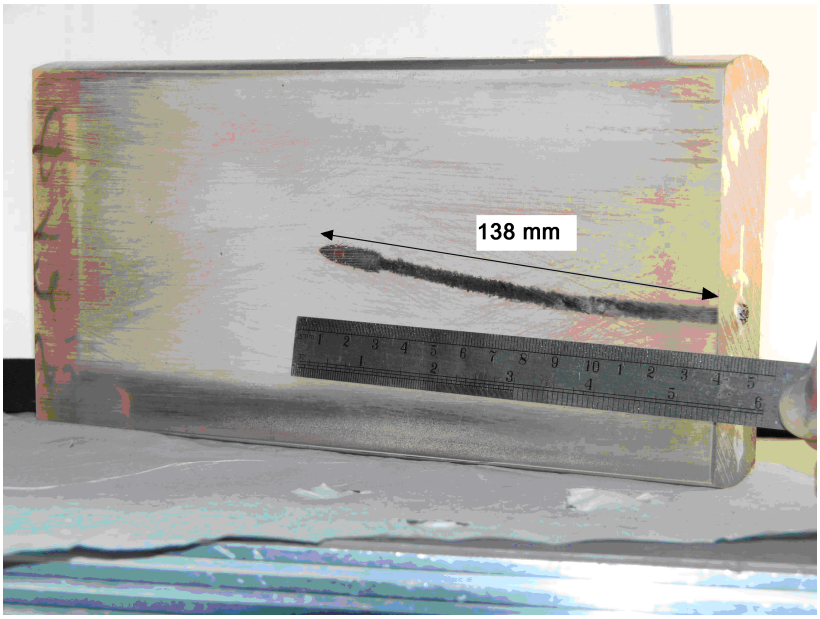

b.

Figure 18 : Normal impact of cylindrical block at 754 m/s. a. The impacted cylinder. b. The trajectory within the cylinder.

4. Summary and Discussion

Inclined ballistic experiments have been conducted in which 7.62 mm armor piercing projectiles impacted thick (50 mm) PC plates at various angles of inclination: 20^o - 80^o. A ricochet was observed for 25^o impact while perforation was observed for all other higher angles. It was observed that the trajectory (for all the cases) consists of three concentric damage zones. The inner zone is a cavity sorrounded by plastic zone which is (approximatly) twice the diameter of the cavity. Attached to the cavity, one observes a narrow cracked zone which is fully embedded within the plastic zone. A significant recovery of the PC is observed. Namely, the diameter of the projectile's core is 6.05 mm while the remaining cavity's diameter is ~ 3-4 mm.

A 3D transient adiabatic numerical analysis was conducted to simulate the ballistic impact using Abaqus commercial software. The Mie-Gruneisen equation of state(EOS) with application of linear U_s-U_p Hugoniot together with Mises plasticity was used for modeling the PC plate. A mesh convergence test was done for the specific geometry and a suitable mesh size of 1.25 mm was chosen and kept constant for all numerical solutions. The combined effects of tensile failure and ductile failure were addressed. The simulations predicted reasonably well the trajectories for different angles of inclination in comparison with the experimental results. Consequently, a numerical investigation of the DOP in PC was carried out. The DOP for impact velocity of 750 m/s was verified experimentally. The discrepancy of 4% which is observed confers reliability

to the numerical model. The penetration velocity is also slightly non-linear with time and the acceleration is almost linear with penetration velocity for all impact velocities. The deceleration is higher at higher velocities. Overall, it must be kept in mind that the numerical results depend on the material and failure properties of the PC at very high strain rates, elevated temperatures and large span of triaxialities. An improved knowledge of these properties is expected to lead to more accurate results. A better material model which includes the recovery and fracture observed in the experiments might also enhance the physical meaning of numerical results. However, given these limitations, this investigation shows that a simplified numerical model can reliably reproduce the main characteristics of the penetration process, thus allowing incorporation into design procedures and experiment planning.

4. Conclusions

The conclusions derived from this investigation can be summarized as follows:

- For an accurate prediction of an impact trajectory within PC plates, sound experimental data of the PC properties and failure envelope (plastic strain at fracture and pressure cutoff) at very high strain rates, high strains, elevated temperatures and large span of triaxialities are still needed.
- The numerical results are mesh dependent and a proper mesh size which fit the experimental results should be identified and used.
- The combined effect of the two failure criteria (tensile vs. ductile failure) can reasonably well predict the projectile trajectory within a thick PC plate, as it was done for thick PMMA plates [14].
- The main contributor to the trajectory within the PC is the "ductile failure with damage evolution" criterion. The effect of "tensile failure" adds up and influences the direction and depth of the projectile.

- The DOP scales slightly non linearly with the projectile's impact velocities and can be approximated by : $DOP\ [mm] = aV_i^2 + bV_i$ where a = 0.000172 , b = 0.06304.
- There is a good agreement between the experimental and numerically calculated DOP for impact velocity of 750 m/s.
- The deceleration during penetration (for all impact velocities) is almost linear with the penetration velocity and is higher for higher velocities.

Acknowledgement

Financial support from PMRI-Technion Security Fund (grant 2011212) and MAFAT-MOD (grant 2013441) is gratefully acknowledged. The authors wish to thank the staff of Rafael Ballistic Laboratory and Mr. Z. Schachar (MMC Technion) for their dedicated technical assistance. .

References

[1] Ravi-Chandar K. On the failure mode transitions in polycarbonate under dynamic mixed-mode loading. Int J Solids Struct 1995; 32: 6-7: 925-938.

[2] Rittel D, Levin R, Maigre H. On dynamic crack initiation in polycarbonate under mixed-mode loading. Mech Res Commun 1997; 24: 1: 57-64.

[3] Rittel D, Levin R. Mode-mixity and dynamic failure mode transitions in polycarbonate. Mech Mater 1998: 30: 3: 197-216.

[4] Rittel D. On the conversion of plastic work to heat during high strain rate deformation of glassy polymers. Mech Mater 1999; 31: 2: 131-139.

[5] Rittel D. Experimental investigation of transient thermoplastic effects in dynamic fracture. Int J Solids Struct 2000; 37: 21: 1 : 2901-2913.

[6] Moisa S, Landsberg G, Rittel D, Halary J L. Hysteretic thermal behavior of amorphous semi-aromatic polyamides. Polym J 2005; 46: 25: 11870-11875.

[7] Sarva S, Mulliken A D, Boyce M C. Mechanics of Taylor impact testing of polycarbonate. Int J Solids Struct 2007; 44: 7-8: 2381-2400.

[8] Wright S C, Huang Y, Fleck N A. Deep penetration of polycarbonate by a cylindrical punch. Mech Mater 1992; 13: 4: 277-284.

[9] Wright S C, Fleck N A, Stronge W J. Ballistic impact of polycarbonate—An experimental investigation. Int J Impact Eng 1993; 13: 1: 1-20.

[10] Li K, Goldsmith W. Perforation of steel and polycarbonate plates by tumbling projectiles. Int J Solids Struct 1997; 34: 35-36: 4581-4596.

[11] Qasim H S, Yousif A A. Effect of distance from the support on the penetration mechanism of clamped circular polycarbonate armor plates. Int J Impact Eng 2008; 35: 11: 1244-1250.

[12] Qasim H S. Impact resistance of a rectangular polycarbonate armor plate subjected to single and multiple impacts. Int J Impact Eng 2009; 36:9: 1128-1135.

[13] Rosenberg Z, Surujon Z, Yeshurun Y, Ashuach Y, Dekel E. Ricochet of 0.3" AP projectile from inclined polymeric plates. Int J Impact Engineering 2005; 31: 221–233.

[14] Dorogoy A, Rittel D, Brill A . A study of inclined impact in polymethylmethacrylate plates. Int J Impact Engng 2010; 37; 285-294

[15] Abaqus/CAE version 6.9-EF1 2009. Dassault Systemes Simulia Corporation, Providence, RI, USA.

[16] Anderson C E. An overview of the theory of hydrocodes. *Int J Impact Engng 1987;*. 5 ; 423-439.

[17] Abaqus/CAE version 6.9-EF1. Abaqus documentation. Abaqus Analysis User's Manual, chapters 20- 21, Dassault systemes. New York: Springer; 2009.

[18] Hazell P J, Roberson C J, Moutinho M. The design of mosaic armour: The influence of tile size on ballistic performance. Mater Des 2008; 29: 1497–1503.

[19] Bauwens-Crowet C, Bauwens J C, Homes G. The temperature dependence of yield of polycarbonate in uniaxial compression and tensile tests. J Mater Sci 1972 ; 7: 176-183.

[20] Rittel D. Dorogoy, A., A methodology to assess the rate and pressure sensitivity of polymers over a wide range of strain rates. J Mech Phys Solids 2008; 56 : 3191–3205.

[21] Fleck N.A., Stronge W.J., Liu J.H. High strain-rate shear response of polycarbonate and polymathyl methacrylate, Proc R Soc Lond A 1990; 429; 459-479.